Revison 1

Low-temperature magnetism of alabandite: crucial role of surface oxidation

J. Cuda[a,*], T. Kohout[b,c,*], J. Filip[a], J. Tucek[a], A. Kosterov[d,e], J. Haloda[f], R. Skala[c], E. Santala[g], I. Medrik[a], R. Zboril[a]

[a]*Regional Centre of Advanced Technologies and Materials, Departments of Physical Chemistry and Experimental Physics, Faculty of Science, Palacky University Olomouc, 17. listopadu 12, 771 46 Olomouc, Czech Republic*

[b]*Department of Physics, University of Helsinki, P.O. Box 64, 00014 Helsinki University, Finland*

[c]*Institute of Geology, Academy of Sciences of the Czech Republic v.v.i., Rozvojová 269, 165 00 Prague, Czech Republic*

[d]*Earth Physics Department, Faculty of Physics, Sanct-Petersburg University, 198504 Peterhoff, Sanct-Petersburg, Russia*

[e]*Resource Center "Geomodel", Sanct-Petersburg University, 198504 Peterhoff, Sanct-Petersburg, Russia*

[f]*Czech Geological Survey, Geologická 6, 152 00 Praha 5, Czech Republic*

[g]*Department of Chemistry, University of Helsinki, P.O. Box 55, 00014 Helsinki University, Finland*

***Corresponding author(s):** e-mail: jan.cuda@upol.cz (Jan Cuda); e-mail: kohout@gli.cas.cz (Tomas Kohout)

Keywords: alabandite (MnS), hausmannite (Mn_3O_4), troilite (FeS), magnetism.

Abstract

Manganese(II) monosulphide crystallizes into three different polymorphs (alpha-, beta-, and gamma-MnS). Out of these, alpha-MnS, also known as mineral alabandite, is considered the most stable and is widespread in terrestrial materials as well as in extraterrestrial objects such as meteorites.

In this study, a low-temperature antiferromagnetic state of alpha-MnS was investigated using macroscopic magnetic measurements as induced and remanent field-cooled (FC) and zero-field-cooled (ZFC) magnetizations and magnetic hysteresis. Both natural alabandite and synthetic samples show (i) Néel temperatures in a narrow temperature range around 153 K and (ii) a rapid increase of the magnetization around 40 K. An anomalous magnetic behavior taking place at about 40 K was previously ascribed to the magnetic transition from a high-temperature antiferromagnetic to a low-temperature ferromagnetic state documented for non-stoichiometric alpha-MnS slightly enriched in manganese. However, our detailed microscopic observations and, in particular, oxidation experiments indicate that the anomalous magnetic behavior around 40 K is caused by a presence of oxide layer of ferrimagnetic hausmannite (Mn_3O_4) on the surface of alpha-MnS rather than being an intrinsic property of nearly stoichiometric alpha-MnS.

1. Introduction

Alabandite is a manganese sulfide with theoretical composition MnS crystallizing in the cubic lattice of galena type (PbS). It occurs as an accessory mineral at many localities worldwide, mainly in epithermal base-metal sulfide veins, in low-temperature manganese deposits [*Doelter*, 1926; *Hewett and Rove*, 1930; *Anthony et al*., 2012] and also in marine sediments [*Lepland and Stevens*, 1998]. Locally, it is an important ore mineral of Mn. Its name is

derived from its supposed discovery locality at Alabanda, Turkey. The type locality of alabandite is Sacarîmb, Romania [*Anthony et al*., 2012].

Apart from terrestrial localities, alabandite is also relatively abundant in certain types of meteorites, e.g., in E chondrites [*Keil*, 1968; *Zhang et al.*, 1995; *Zhang and Sears*, 1996; *Brearley and Jones*, 1998] and related achondritic aubrites [*Keil and Fredriksson*, 1967; *Ryder and Murali*, 1987; *Lin et al.*, 1989; *Mittlefehldt et al*., 1998]. It was also reported in some ureilites [*Fioretti and Molin*, 1998] and winonaites [*Mason and Jarosewich*, 1967].

Alabandite is paramagnetic at room temperatures and orders antiferromagnetically below its Néel temperature T_N ~148 K [*Heikens et al*., 1977]. A slightly higher T_N (~153 K) was later published by *Pearce et al.* [2006]. A structural transition occurs at T ~130 K which is interpreted as an abrupt inversion of the rhombohedral distortion of the f.c.c. lattice along [1 1 1] plane accompanied by a discontinuous change in the magnetic susceptibility observed in alabandite single crystals [*Heikens et al*., 1977].

Magnetic susceptibility and induced field-cooled and zero-field-cooled magnetization (in 10 mT of external magnetic field) of antiferromagnetic alabandite below its T_N are low, typically in the range of 10^{-7} m^3/kg and 3-4 mAm^2/kg, respectively. The substitution of Mn^{2+} ions by Fe^{2+} has a pronounced effect on the Néel temperature which increases with increasing iron content reaching ~185 K for the $Fe_xMn_{1-x}S$ system with x = 0.2 [*Petrakovski et al.*, 2002]. Still more iron-rich alabandite samples (x > 0.25) exhibit ferrimagnetic behavior above room temperature with Curie temperatures T_C between 730 K (x = 0.27) and 860 K (x = 0.38) [*Loseva et al*., 1998; *Petrakovski et al.*, 2002]. However, magnetization of this ferrimagnetic-ordered alabandite is weak, close to that of paramagnetic MnS.

It was reported that iron-free MnS samples with a slight excess of Mn show antiferro- to ferromagnetic transition at T ~40 K [*Petrakovski et al.*, 2001]. This transition manifests itself in a sharp, two orders of magnitude, increase of induced magnetization on cooling. Such a

sharp change in magnetic properties can significantly increase magnetic response of alabandite at low temperatures and can potentially contribute to low-temperature magnetic properties of extraterrestrial bodies [*Kohout et al.*, 2010]. Similar low-temperature magnetic transition is observed in troilite (FeS) [*Kohout et al.*, 2007; *Cuda et al.*, 2011]. Moreover, *Gattacceca et al.* [2011] recently reported that chromite with Curie temperature in the 40–80 K range exist in certain meteorites and may significantly modify their low-temperature magnetic properties. Therefore, verification, interpretation and quantification of this magnetic phenomenon in alabandite samples and its comparison to low-temperature magnetic properties of troilite and chromite are required and are the subject of this study.

2. Materials and methods

Basic characteristics of our samples are summarized in the Table 1. Natural polycrystalline sample of alabandite (NA) originates from Broken Hill, N.S.W., Australia, sample Bm 1972, 294, kindly provided by Natural History Museum, London. Additionally, nearly stoichiometric alpha-MnS was synthesized adopting two alternative procedures.

SA1 sample was prepared using a slightly modified solvothermal process of *Biswas and Chaudhuri* [2007]. First, manganese acetate [$(CH_3CO_2)Mn{\cdot}4H_2O$, purity >99.0%, Sigma Aldrich] and thiourea [CH_4N_2S, purity >99.0%, Sigma Aldrich] was mixed in a molar ratio of 1:3 with a water solvent, loaded into an ace pressure tube (Sigma Aldrich) and placed into a furnace at 190˚C for 17 hours. Subsequently dried product was annealed in a helium atmosphere at temperatures up to 450˚C.

SA2 sample was synthesized by direct thermal fusion of sulfur (purity >98.0%, Sigma Aldrich) and manganese (purity >99.0%, Sigma Aldrich) powders in stoichiometric molar ratio. The precursors were annealed twice in a sealed quartz tube under reduced pressure for 12 hours at 700°C including sample homogenization between two subsequent runs.

Measurements of the macroscopic magnetic response such as induced and remanent field-cooled (FC) and zero-field-cooled (ZFC) magnetizations and magnetic hysteresis measurements were carried out at the Institute for Rock Magnetism, University of Minnesota and at the Regional Centre of Advanced Technologies and Materials, Palacky University Olomouc, using MPMS5S and MPMS XL-7 (both Quantum Design) SQUID magnetometers. Details of FC and ZFC measurement procedure are provided in auxiliary material.

X-Ray Diffraction (XRD) patterns of all samples were recorded with a PANalytical X'Pert PRO MPD diffractometer (iron-filtered CoK_α radiation: λ = 0.178901 nm, 40 kV and 30 mA) in the Bragg-Brentano geometry. Samples were placed on a zero-background Si slides and scanned in a continuous mode (resolution of 0.017 ° 2 Theta, scan speed of 0.0016 ° 2 Theta per second). Identification of crystalline phases and Rietveld refinements were obtained using the software High Score Plus (PANalytical) in conjunction with the PDF-4+ and ICSD databases (ICSD collection codes: MnS – 41331, Mn_3O_4 – 31094, Mn_2O_3 – 76087, S – 63082). Peak shapes were modeled using the pseudo-Voigt function, separately refining the Caglioti parameters (u, v, w), unit cell parameters, and scale factor for each phase.

Bulk chemical composition of the SA2 sample was determined using a quantitative X-ray wavelength dispersive spectral analysis on a MICROSPEC 3PC X-ray wavelength dispersive system (WDS) on a CamScan 3200 scanning electron microscope (SEM) at the Czech Geological Survey. The analyses were performed using an accelerating voltage of 20 kV, 25 nA beam current, 1 μm beam size and ZAF correction procedures. The counting times were 30 s for all analyzed elements. A combination of natural and synthetic standards was used for calibration.

SEM TESCAN VEGA 3XM at Institute of Geology, Academy of Sciences of the Czech Republic has been used to document surface features of the natural alabandite (NA sample). To avoid potential deterioration of the sample, the specimen has not been coated and the SEM

has been operated at low-vacuum mode. Energy dispersive x-ray (EDX) spectra of individual phases observed on the surface of the studied specimen have been acquired with a Bruker XFlash detector. Subsequently, part of the sample has been polished and analyzed with an electron microprobe (EMPA) CAMECA SX-100 instrument at the Institute of Geology, Academy of Sciences of the Czech Republic to determine the stoichiometry of the sample interior.

3. Results and discussion

3.1. Characterization and low-temperature magnetic properties of alpha-MnS

XRD patterns of a natural alabandite (NA) and of two synthetic alpha-MnS (SA1 and SA2) samples are shown in Figure 1a, 1b, and 1c. They perfectly correspond to the cubic structure of alpha-MnS (PDF No. 01-088-2223). In the NA sample, some amount of elemental sulfur (16% by Rietveld refinement) and hausmannite (see below) has been found in addition to the alabandite main phase. The presence of sulfur on NA sample surface was also confirmed by SEM/EDX (Figure S1 of the auxiliary material). In contrast, EMPA of the NA sample interior did not reveal any presence of sulfur or hausmannite. SEM-WDS analysis of the SA2 sample show similar result. Based on the information provided above, all three studied samples can be considered as a representative of alabandite with only a minor presence of other phases limited to the surface of the individual grains.

Temperature dependence of induced FC and ZFC magnetizations at 10 mT (Figure 2) as well as remanent FC and ZFC magnetizations (imprinted by 2.5 T at 5 K, Figure 3) yield Néel temperatures (T_N) for natural and synthetic samples in a narrow temperature range around 153 K as expected for alabandite [*Pearce et al.*, 2006]. Néel temperature manifests itself through peaks on the induced magnetization curves, and through merging of the FC and ZFC remanent magnetization curves at T_N.

In all alabandite samples, a feature at 40 ± 2 K is further observed, manifested through a rapid increase of magnetic response with decreasing temperature (Figure 2 and 3). Enhanced magnetic response is also seen in the hysteresis properties at 5 K, namely, an S-shaped hysteresis loop and a tendency to saturation in high external magnetic field (Figure 4). Such behavior is typical for the ferro/ferrimagnetic materials rather than for an antiferromagnetic one.

Enhanced magnetic response below 40 ± 2 K is similar to that reported for iron-free alpha-MnS samples slightly enriched in Mn with respect to a stoichiometric alpha-MnS and interpreted as an antiferro- to ferromagnetic transition at 40 K upon cooling [*Petrakovski et al*. 2001]. However, in our case both NA and SA2 samples are highly stoichiometric examples of alabandite (Table 1). According to our measurements, the enhanced magnetic response at around 40 K occurs in all studied samples and its amplitude does not correlate with Mn/S ratio. Thus, a question arises whether such low-temperature behavior is limited to alabandite samples slightly enriched in Mn as reported by *Petrakovski et al*. [2001], or it is a general phenomenon occurring in stoichiometric or Mn-depleted alabandite samples as well. Alternatively, a presence of small amounts of another phase on alabandite grain surfaces identified above may be responsible for the observed low-temperature magnetic behavior and will be evaluated in following section.

3.2. Effects of surface oxidation on low-temperature magnetic properties of alpha-MnS

In order to confirm or exclude the role of manganese oxides on the magnetic response of alpha-MnS (sulfur should not significantly influence the low-temperature magnetic properties of alabandite), we artificially oxidized the SA1 sample by hydrogen peroxide (H_2O_2). About 20 mg of SA1 material was briefly submerged in hydrogen peroxide and air-dried at room temperature for 20 hours (sample labeled as SA1_OX). Subsequently, XRD and magnetic

175 measurements were carried out following the same procedures as for other samples (Figures
176 1d and 5).

177 Upon hydrogen peroxide treatment, surface of MnS was partially oxidized into manganese
178 oxide phases and thus the ratio of alabandite to manganese oxides in the SA1_OX sample
179 changed compared to original SA1 sample. Presence of manganese oxide Mn_3O_4, known also
180 as mineral hausmannite, was confirmed by XRD analysis in the SA1_OX sample (Figure 1d).
181 Hausmannite has Curie temperature T_C ~41 ÷ 43 K [*Dwight and Menyuk*, 1960; *Robie and*
182 *Hemingway*, 1985]. It is very close to the temperature where enhanced magnetic response of
183 alabandite is observed upon cooling, making hausmannite a meaningful candidate to explain
184 the observed low-temperature magnetic behavior of alabandite. Other phases identified in the
185 XRD pattern are bixbyite (alpha-Mn_2O_3, antiferromagnetic below 80 K [*Robie and*
186 *Hemingway*, 1985] or 90 K [*Mukherjee et al.*, 2006]) and sulfur (diamagnetic [*O'Handley*,
187 2000; *Blundell*, 2001]). These phases do not have any magnetic transitions around 40 K which
188 would explain observed magnetic behavior at this temperature.

189 Oxidized SA1_OX sample shows a significant (by a factor of eight) increase in its magnetic
190 response below 40 ± 2 K compared to the unoxidized alpha-MnS sample (insets in Figure 5).
191 Dependence of magnitude of the 40 K magnetic response on the amount of manganese
192 oxides, including hausmannite, suggests that the low-temperature behavior observed in
193 studied alabandite samples is not an intrinsic property of alabandite itself, but rather
194 hausmannite governs the low-temperature magnetic response below ~40 K. Similar example
195 was described for antiferromagnetic MnO nanoparticles with Mn_3O_4 surface layers [*Berkowitz*
196 *et al.*, 2008].

197 Assuming that ferromagnetic-like hysteresis loops measured at 5 K are produced entirely by
198 Mn_3O_4, it is possible to estimate its content in the studied samples. However, caution is
199 needed when interpreting the hysteresis data, since, unlike many other compounds of spinel

type, Mn_3O_4 does not reach magnetic saturation even in fields as high as 34 T [*Nielsen and Roeland*, 1976]. Corresponding saturation magnetization value, determined from extrapolation to zero magnetic field of the magnetization field dependence measured along [010] direction, amounts to 47.2 Am^2/kg. Experiments performed in much lower maximum fields, which are more appropriate to compare with ours, yielded respectively lower values of the high-field magnetization extrapolated to zero field (M_E): 34.2 Am^2/kg (1.4 Bohr magnetons per formula unit) for the 1 T field [*Wickham and Croft*, 1958] and 38.1 Am^2/kg (1.56 Bohr magnetons per formula unit) for the 14 T field [*Jacobs*, 1959].

For our experiments, carried out in the 7 T maximum field, we adopted an intermediate value of 36 Am^2/kg. M_E of the SA1_OX sample (i.e., after oxidation) amounts to 7.3 Am^2/kg at 5 K (Table 2) corresponding to a presence of ~20 wt.% of hausmannite. This is in a reasonably good accordance with the result of Rietveld refinement where the amount of hausmannite in this oxidized sample appears to be 22.9(4) wt.%. The remaining difference may be due to a small size of at least a fraction of hausmannite grains as suggested by broad diffraction peaks of hausmannite in the XRD pattern (Figure 1d; see also *Siskova et al*., 2012 and *Markova et al.*, 2012). Indeed, nanosized Mn_3O_4 shows considerably reduced M_E values as determined from hysteresis loops measured in maximum fields up to 7 T [*Winkler et al.*, 2004, *Vázquez-Olmos et al.*, 2005].

We expect that hausmannite governs the magnetic response below 40 K in other studied samples as well. Comparing, as above, the M_E values at 5 K (Table 2) with the Mn_3O_4 M_E bulk value of 36 Am^2/kg, we can estimate the hausmannite content. Approximately 2.4 wt.%, 0.1 wt.%, and 5.3 wt.% of hausmannite are required to produce the low-temperature magnetic response observed in SA1 (before oxidation), SA2, and natural alabandite (NA) samples, respectively. These values are close to, or below, the detection limit of XRD measurements

and thus not observed in the XRD pattern of these samples except for NA sample (6.9(4) wt.% of Mn_3O_4 as calculated using Rietveld refinement).

Furthermore, a profile of the temperature-dependent induced FC magnetization curve of samples NA, SA1 and especially SA1_OX displays a tendency to follow the Curie-Weiss law above 40 K. The hysteresis loops below 40 K show also shift along field (horizontal) axis towards negative values (compare Bc+ and Bc- in Table 2) which seems to be a manifestation of exchange interaction between antiferromagnetic and ferro- or ferrimagnetic phases [Nogues and Schuller, 1999]. Exchange bias or exchange anisotropy is present in bi-layers (or multi-layers) of magnetic materials which in our case are represented by alabandite (antiferromagentic) and hausmannite (ferrimagentic). On the other hand, we cannot exclude a random canting of the particle surface spins caused by competing antiferromagnetic exchange interactions at the surface of hausmannite particles producing exchange anisotropy between their core and surface spins.

In the SA2 sample with an extremely low (~0.1%) hausmannite content, the magnetic signal above 40 K does not show a tendency to follow the Curie-Weiss law, and the low-temperature behavior is dominated by a stronger alabandite antiferromagnetic response than a paramagnetic behavior of Mn_3O_4 present in the oxidized surface layer of alabandite grains.

Upon heating in the temperature range between T_C of hausmannite and T_N of alabandite, the decreasing paramagnetic response of hausmannite overlaps with the slightly increasing antiferromagnetic response of alabandite. A local minimum in the induced FC curve can be observed in this temperature range and it is shifted to the higher temperatures with increasing hausmannite content (insets in Figure 2). In this case, it appears that there is a direct correlation between the amount of hausmannite present in the sample and temperature at which the minimum occurs. The estimated temperatures are 44 ± 1 K, 89 ± 1 K and 146 ± 1 K for SA2, SA1, and NA samples, respectively, and follow positive trend with increasing

hausmannite content. For sample SA1_OX, we do not observe the minimum in temperature range from 40 to 155 K because the paramagnetic response of hausmannite (and perhaps also of bixbyite) dominates over the antiferromagnetic response of alpha-MnS.

Last but not least, the temperature dependence of induced ZFC measurements of NA, SA1, SA2 and SA1_OX samples exhibits a sharp peak below the Curie temperature ascribed to hausmannite, and then on subsequent heating drops down to a very low values (Figures 2 and 5a). The observed peak can be interpreted as a Hopkinson peak observed just prior to transition from magnetically ordered state to a paramagnetic one [*Dunlop and Özdemir,* 1997] rather than as an effect accompanying a magnetic transition from ferromagnetic to a antiferromagnetic state as suggested by *Petrakovski et al.* [2001].

The positive correlation between Mn enrichment and magnitude of the 40 K feature observed in synthetic alabandite by *Petrakovski et al.* [2001] can be explained as the extra Mn added did not enter alabandite structure and rather reacted with oxygen to produce manganese oxides including hausmannite. Thus, higher addition of Mn resulted in higher production of hausmannite causing higher amplitude of the 40 K feature.

3.3. Comparison to other low-temperature magnetic minerals

Similar low-temperature magnetic transition, as described above in alabandite – hausmannite system, is observed at ~70 K in other sulfur monosulfide – troilite FeS [*Kohout et al.*, 2007; *Cuda et al.*, 2011]. *Gattacceca et al.* [2011] recently reported that chromite with Curie temperature in 40-80 K range exists in certain meteorites and chromite contamination within troilite samples may be responsible for the observed ~70 K feature in troilite. In this respect alabandite with hausmanite contamination is analogue to troilite with proposed chromite contamination. Thus, in following paragraph we briefly compare alabandite – hausmannite system to the troilite and chromite.

At the first look both systems show very similar behavior with a sharp increase in both induced and remanent magnetization and onset of ferromagnetic-like hysteresis below the transition temperature. The difference between these two systems is in nature of the contaminant. Hausmannite is of similar composition to alabandite (both manganese bearing phases) and is localized at the surface of alabandite grains. Thus it can be easily overlooked in EMPA analysis of polished grains. In contrast, chromite contamination is supposed to be present within the interior of troilite grains and thus should be more easily observable. Thorough analytical data (EMPA and SEM-BSE (BackScattered Electrons) observation of polished grain sections, AAS (Atomic Absorption Spectroscopy), XRD and Mössbauer spectroscopy of bulk troilite samples in *Cuda et al.* [2011]) reveal chromium content one to three orders of magnitude lower than predicted for chromite amount explaining low-temperature magnetic observations. Another difference can be observed on induced ZFC magnetization curves. While in alabandite – hausmannite case the ZFC induced magnetization stays well below FC and shows a pronounced Hopkinson peak just below T_C of hausmannite (Figure 2), the ZFC curve of troilite do not show obvious presence of Hopkinson peak (Figure 3 in *Kohout et al.* [2007]). Thus, the nature of the contaminant or mechanism of the low-temperature transition in troilite is likely to be different than proposed chromite (or similar to alabandite – hausmannite case).

4. Conclusions

Based on our detailed investigation, the low-temperature phenomenon at ~40 K, previously observed in some synthetic alabandite samples and ascribed to nonstoichiometry of the latter, is not the intrinsic property of alabandite. It appears to be a result of ferri- to paramagnetic transition of hausmannite (Mn_3O_4) present in oxidized surface layer on crystals/grains of alabandite. Presence of hausmannite even in amounts below 1 wt.% can have a detectable

299 effect on magnetic response of alabandite, which is otherwise a purely antiferromagnetic
300 material below its Néel temperature of ~153 K without any other low-temperature magnetic
301 transitions. This conclusion rules out pristine alabandite to significantly contribute to
302 remanent or induced magnetism of minor Solar System bodies. In contrary, no prove of
303 similar contamination has been found in troilite showing similar transition ~70 K.
304

305 **Acknowledgments**

306 The authors gratefully acknowledge the support by the Grant Agency of the Academy of
307 Sciences of the Czech Republic (KJB300130903), Institute of Geology ASCR, v.v.i., research
308 project (RVO67985831), Czech Science Foundation (GACR P108/11/1350), the internal
309 grant of Palacky University in Olomouc, Czech Republic (PrF_2013_014) and the
310 Operational Program Research and Development for Innovations - European Regional
311 Development Fund (CZ.1.05/2.1.00/03.0058 of the Ministry of Education, Youth and Sports
312 of the Czech Republic) and by a Visiting Fellowship at the Institute for Rock Magnetism,
313 which is funded by the Instruments & Facilities program of the National Science Foundation.
314 We also thank Vlasta Böhmova and Zuzana Korbelova for their assistance with SEM/EDX,
315 EPMA analyses and Zdenka Markova for her assistance with MnS sample preparation.
316
317
318
319
320
321
322
323

References

Anthony, J.W., Bideaux, R.A., Bladh, K.W., Nichols M.C., Eds., Handbook of Mineralogy, Mineralogical Society of America, Chantilly, VA 20151-1110, USA. http://www.handbookofmineralogy.org/ (viewed 13.1.2012).

Berkowitz, A.E., Rodriguez, G. F., Hong, J. I., An, K., Hyeon, T., Agarwal, N., Smith D.J., and Fullerton E.E. (2008) Antiferromagnetic MnO nanoparticles with ferrimagnetic Mn_3O_4 shells: Doubly inverted core-shell system. Physical Review B, 77, 024403, doi: 10.1103/PhysRevB.77.024403.

Biswas, S., Kar, S., and Chaudhuri, S., (2007) Growth of different morphological features of micro and nanocrystalline manganese sulfide via solvothermal process. Journal of Crystal Growth, 299, 94-102, doi: 10.1016/j.jcrysgro.2006.10.236.

Blundell, S. (2001) Magnetism in Condensed Matter, Oxford Univ. Press Inc., New York.

Brearley, A. J. and Jones, R.H. (1998) Chondritic meteorites. In Papike, J. J. (ed.) Planetary materials. Reviews in Minaralogy, 36, p. 3-264. Mineralogical Society of America.

Cuda, J., Zboril, R., Schneeweiss, O., Tucek, J., Prochazka, V., Maslan, and M., Tucek, P. (2010) Mössbauer study and macroscopic/global magnetic behavior of powdered ilmenite ($FeTiO_3$) sample. In Mössbauer Spectroscopy in Materials Science: 2010, AIP Conference Proceedings, vol. 1258, edited by J. Tucek and M. Miglierini, pp. 55–67, American Institute of Physics, Melville, N. Y.

Cuda, J, Kohout, T., Tucek, J., Haloda, J., Filip, J., Prucek, R., and Zboril, R. (2011) Low-temperature magnetic transition in troilite: A simple marker for highly stoichiometric FeS systems. Journal of Geophysical Research, 116, B11205, doi: 10.1029/2011JB008232.

Doelter, C. (1926) Handbuch der Mineralchemie, 4(1), 485.

Dunlop, D.J. and Özdemir, Ö. (1997) Rock Magnetism Fundamentals and frontiers. Cambridge University Press, Cambridge.

Dwight, K. and Menyuk, N. (1960) Magnetic properties of Mn_3O_4 and the canted spin problem. Physical Review, 119, 1479-1479, doi: 10.1103/PhysRev.119.1470.

Fioretti, A. M. and Molin, G. (1998) Alabandite in ureilite Frontier Mountain 95028. Meteoritics and Planetary Science, 33(4), A46-47.

Gattacceca, J., Rochette, P., Lagroix F., Mathé, P.E., and Zanda, B. (2011) Low temperature magnetic transition of chromite in ordinary chromites. Geophysical Research Letters, 38, L10203, doi: 10.1029/2011GL047173.

Heikens, H.H., Wiegers, G.A., and Van Bruggen, C.F. (1977) On the nature of a new phase transition in α-MnS. Solid State Communications, 24, 205-209.

Hewett, D. F. and Rove, O. N. (1930) Occurrence and relations of alabandite. Economic Geology, 25(1), 36-56.

Jacobs, I.S. (1959) Evidence for triangular moment arrangements in MO • Mn_2O_3. Journal of Physics and Chemistry of Solids, 11, 1-11.

Keil, K. (1968) Mineralogical and Chemical Relationships among Enstatite Chondrites. Journal of Geophysical Research, 73(22), 6945–6976, doi: 10.1029/JB073i022p06945.

Keil, K., Fredriksson, K. (1967) Electron microprobe analysis of some rare minerals in the Norton County achondrite. Geochimica et Cosmochimica Acta, 27(9), 939-942, doi: 10.1016/0016-7037(63)90103-0.

Kohout T., Kosterov, A., Haloda, J., Týcová, , P, Zbořil R (2010) Low temperature magnetic properties of iron bearing sulfides and their contribution to magnetism of cometary bodies. Icarus, 208, 955-962, doi: 10.1016/j.icarus.2010.03.021.

Kohout, T., Kosterov, A., Jackson, M., Pesonen, L.J., Kletetschka, G., and Lehtinen, M., (2007) Low-temperature magnetic properties of the Neuschwanstein EL6 meteorite. Earth and Planetary Science Letters, 261, 143–151, doi: 10.1016/j.epsl.2007.06.022.

373 Lepland, A. and Stevens, R.L. (1998) Manganese authigenesis in the Landsort Deep, Baltic
374 Sea. Marine geology, 151(1-4), 1-25, doi: 10.1016/S0025-3227(98)00046-2.
375 Lin, Y. T., El Goresy, A., and Hutcheon, I.D. (1989) The First Meteoritic Silver Minerals in
376 Pena Blanca Springs Enstatite Achondrite: Assemblages, Compositions and Silver
377 Isotopes. Twentieth Lunar and Planetary Science Conference (1989), Abstract #1291.
378 Loseva, G.V., Ryabinkina, L.I., and Balaev, A.D. (1998) Ferromagnetism and the metal–
379 insulator transition in the magnetic semiconductor system $Fe_xMn_{1-x}S$. Physics of the Solid
380 State, 40, 250–251 (Translated from Fizika Tverdogo Tela 40, 276–277).
381 Markova, Z., Šišková, K., Filip, J., Šafářová, K., Prucek, R., Panáček, A., Kolář, M., and
382 Zbořil, R. (2012) Chitosan-based synthesis of magnetically-driven nanocomposites with
383 biogenic magnetite core, controlled silver size, and high antimicrobial activity. Green
384 Chemistry, 14, 2550-2558.
385 Mason, B., and Jarosewich, E. (1967) The Winona meteorite. Geochimica et Cosmochimica
386 Acta, 31(6), 1097-1099, doi: 10.1016/0016-7037(67)90083-X.
387 Mittlefehldt, D.W., McCoy, T.J., Goodrich, and C.A., Kracher A. (1998) Non-chondritic
388 meteorites from asteroidal bodies. In Papike, J. J. (ed.) Planetary materials, Reviews in
389 Minaralogy, 36. Mineralogical Society of America, p. 4-99.
390 Mukherjee, S., Pal A.K., Bhattacharya S., and Raittila J. (2006) Magnetism of Mn_2O_3
391 nanocrystals dispersed in a silica matrix: Size effects and phase transformations. Physical
392 Review B, 74, 104413, doi: 0.1103/PhysRevB.74.104413.
393 Nielsen, O.V., and Roeland, L.W. (1976) High-field magnetization for Mn_3O_4 single crystals.
394 Journal of Physics C: Solid State Physics, 9, 1307-1311.
395 Nogues, J., and Schuller J.K. (1999) Exchange bias. Journal of Magnetism and Magnetic
396 Materials, 192, 203-232, doi: 10.1016/S0304-8853(98)00266-2.

O'Handley, R.C. (2000) Modern Magnetic Materials Principles and Applications .John Wiley & Sons, Inc., New York.

Pearce, C.I., Pattrick, R.A.D., and Vaughan, D.J. (2006) Electrical and Magnetic Properties of Sulfides. Reviews in Mineralogy and Geochemistry, 61, 127-180, doi: 10.2138/rmg.2006.61.3.

Petrakovski, G.A., Ryabinkina, L.I., Abramova, G.M., Velikanov, D.A., and Bovina, A.F., (2001) Antiferromagnet–ferromagnet transition in α-Mn_xS manganese sulfides. Physics of the Solid State, 43, 493–495 (Translated from Fizika Tverdogo Tela 43, 474–476).

Petrakovski, G.A., Ryabinkina, L.I., Abramova, G.M., Balaev, A.D., Romanova, O.B., and Makovetski, G.I. (2002) Magnetic properties of $Fe_xMn_{1-x}S$ sulfides exhibiting the magnetoresistive effect. Physics of the Solid State, 44, 1925–1928 (Translated from Fizika Tverdogo Tela 44, 1836–1839).

Robie R.A. and Hemingway, B.S. (1985) Low-temperature molar heat capacities and entropies of MnO_2 (pyrolusite), Mn_3O_4 (hausmannite), and Mn_2O_3 (bixbyite). The Journal of Chemical Thermodynamics, 17, 165-181.

Ryder, G. and Murali, A.V. (1987) Mineralogy and Chemistry of Antarctic Aubrites. Meteoritics, 22, 495-496.

Siskova, K., Tucek, J., Machala, L., Otyepkova, E., Filip, J., Safarova, K., Pechousek, J., and Zboril, R. (2012) Air-stable nZVI formation mediated by glutamic acid: solid-state storable material exhibiting 2D chain morphology and high reactivity in aqueous environment. Journal of Nanoparticle Research, 14, 805.

Vázquez-Olmos, A., Redón, R., Mata-Zamora, M.E., Morales-Leal, F., Fernández-Osorio, A.L., and Saniger, J.M. (2005) Structural and Magnetic study of Mn_3O_4 Nanoparticles. Reviews on Advanced Materials Science, 10, 362-366.

Wickham, D.G. and Croft, W.J. (1958) Crystallographic and magnetic properties of several spinels containing trivalent manganese. Journal of Physics and Chemistry of Solids, 7, 351-360.

Winkler, E., Zysler, R.D., and Fiorani, D. (2004) Surface and magnetic interaction effects in Mn_3O_4 nanoparticles. Physical Review B, 70, 174406-5.

Zhang, Y. and Sears, D.W.G. (1996) The thermometry of enstatite chondrites: A brief review and update. Meteoritics, 31, 647-655.

Zhang, Y., Benoit, P.H., and Sears, D.W.G. (1995) The classification and complex thermal history of the enstatite chondrites. Journal of Geophysical Research, 100(E5), 9417–9438, doi:10.1029/95JE00502.

435 **Figure captions**

436 **Figure 1** XRD patterns of the samples: (a) NA, (b) SA1, (c) SA2, and (d) SA1_OX. Result of
437 the Rietveld refinement of SA1_OX sample is: 24.0(2) wt.% of MnS, 23(1) wt.% of Mn_3O_4,
438 22.9(4) wt.% of Mn_2O_3, and 30(1) wt.% of sulfur. The respective PDF cards shown below
439 XRD patterns are: 1 - 01-088-2223 (MnS); 2 - 01-075-1560 (Mn_3O_4); 3 - 01-089-4836
440 (Mn_2O_3); 4 - 01-078-1888 (S).

441

442 **Figure 2** Induced-ZFC and FC magnetization curves in the external magnetic field of 10 mT
443 for samples: (a) NA, (b) SA1 and (c) SA2.

444

445 **Figure 3** ZFC-FC curves of remanent magnetization imprinted by a field of 2.5 T for
446 samples: (a) NA and (b) SA1.

447

448 **Figure 4** Hysteresis loops of samples: (a) NA, (b) SA1 and (c) SA2, measured at 5 K (the
449 high-field slope has been subtracted).

450

451 **Figure 5** (a) Induced-ZFC and FC magnetization curves in the external magnetic field of
452 10 mT for SA1_OX sample. Induced-FC curves of the SA1 sample before and after oxidation
453 are displayed for comparison in the inset. (b) ZFC-FC curves of remanent magnetization
454 imprinted by a field of 2.5 T for the SA1_OX sample. Remanent-FC curves of the SA1 before
455 and after oxidation are displayed for comparison in the inset. (d) Hysteresis loops of the SA1
456 sample before and after oxidation at 5 K after slope correction.

457

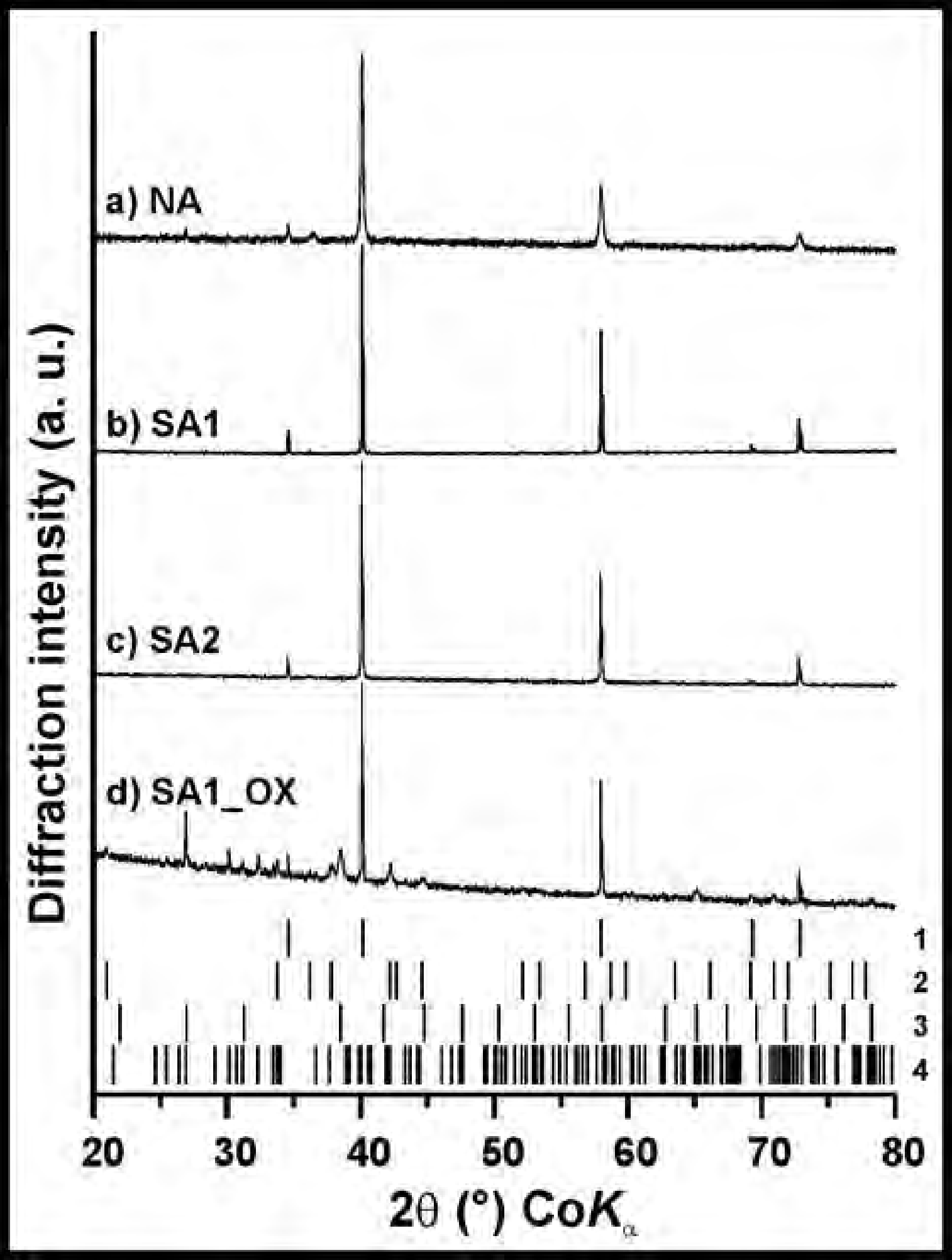
a) NA
b) SA1
c) SA2
d) SA1_OX
Diffraction intensity (a. u.)
1
2
3
4
20
30
40
50
60
70
80
2θ (°) CoK$_\alpha$

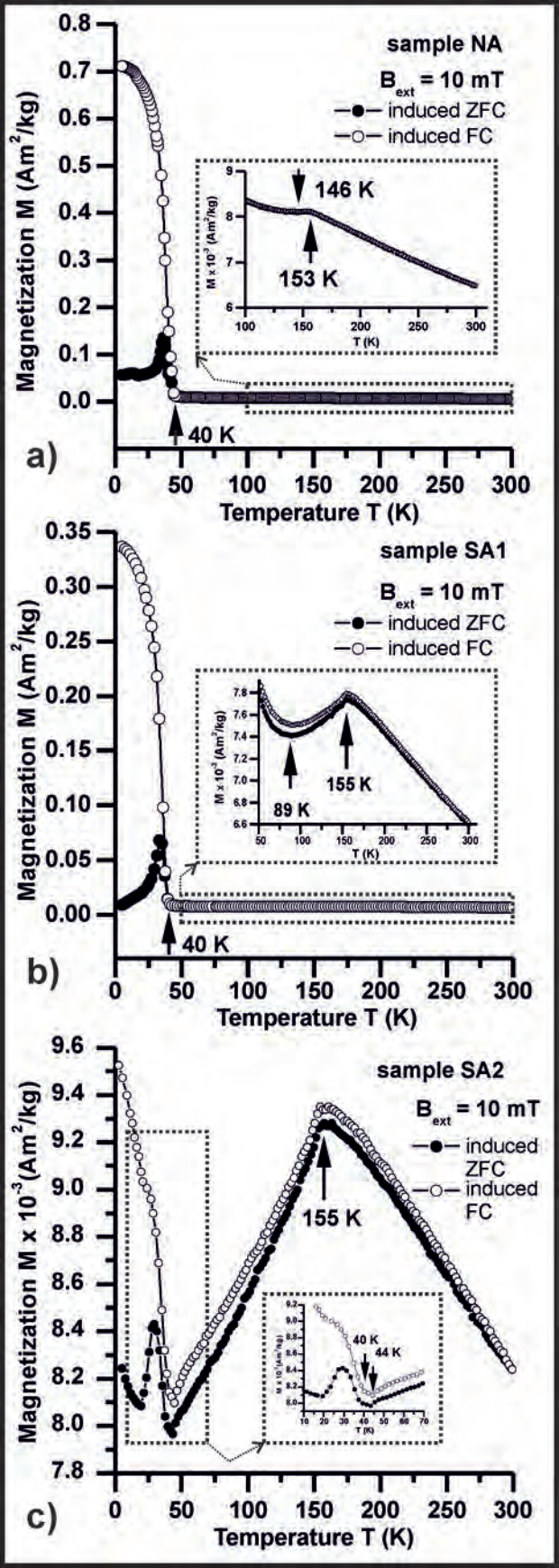
sample NA
B_ext = 10 mT
induced ZFC
induced FC
146 K
153 K
40 K
Magnetization M (Am²/kg)
Temperature T (K)
a)
sample SA1
B_ext = 10 mT
induced ZFC
induced FC
155 K
89 K
40 K
Magnetization M (Am²/kg)
Temperature T (K)
b)
sample SA2
B_ext = 10 mT
induced ZFC
induced FC
155 K
40 K
44 K
Magnetization M x 10⁻³ (Am²/kg)
Temperature T (K)
c)

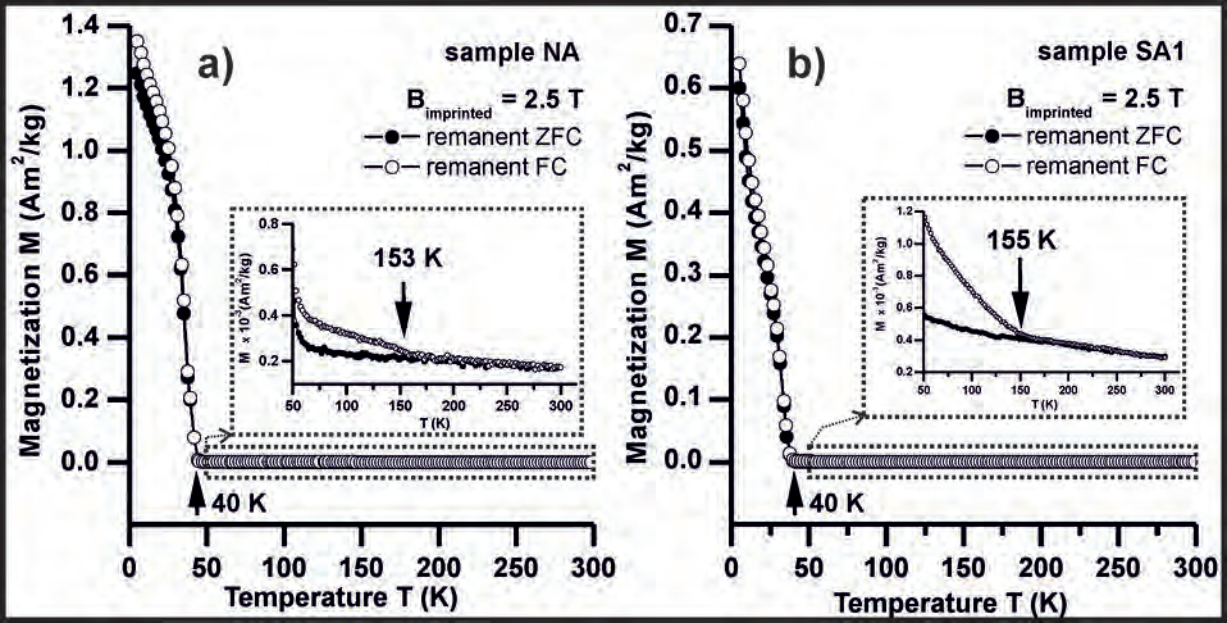
a)
sample NA
B imprinted = 2.5 T
remanent ZFC
remanent FC
153 K
40 K
Magnetization M (Am²/kg)
Temperature T (K)
M x 10⁻³ (Am²/kg)
T (K)
b)
sample SA1
B imprinted = 2.5 T
remanent ZFC
remanent FC
155 K
40 K
Magnetization M (Am²/kg)
Temperature T (K)
M x 10⁻³ (Am²/kg)
T (K)

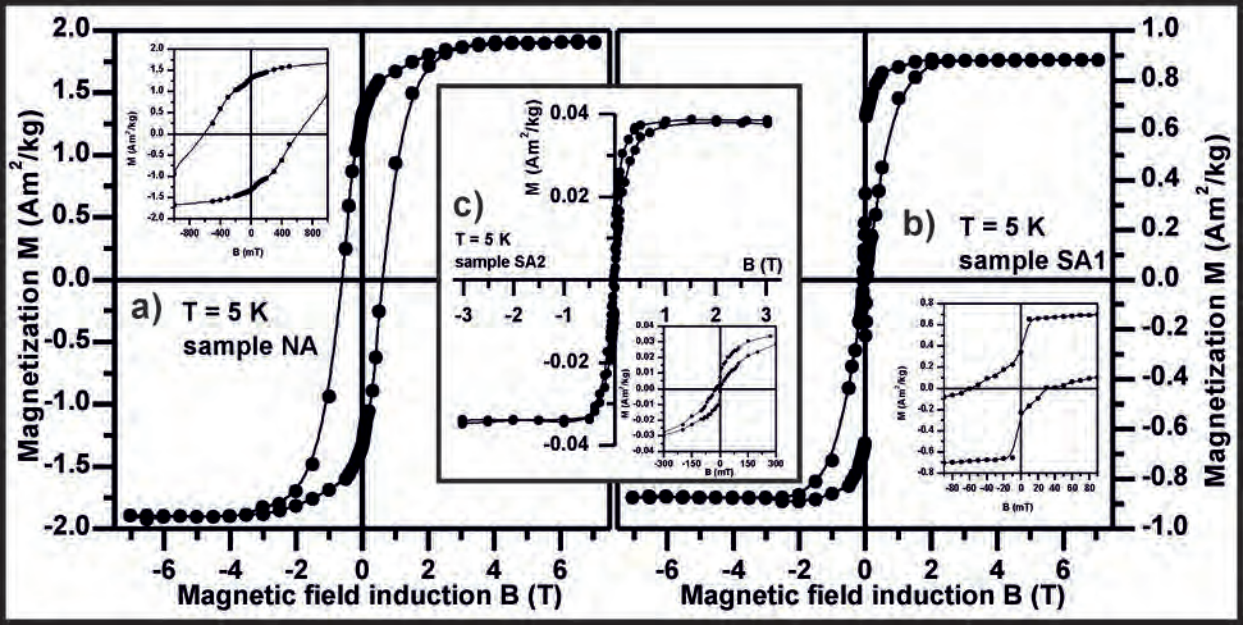
a) T = 5 K
sample NA
b) T = 5 K
sample SA1
c)
T = 5 K
sample SA2
Magnetization M (Am²/kg)
Magnetic field induction B (T)
B (T)
M (Am²/kg)

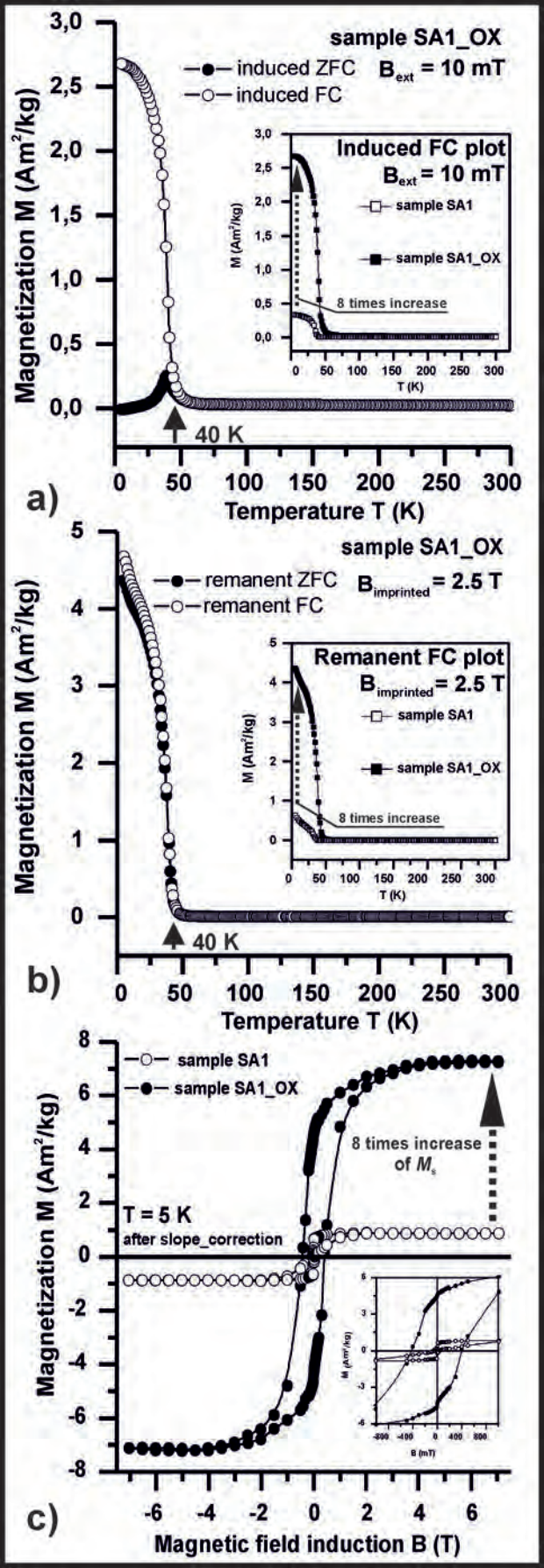
sample SA1_OX
induced ZFC
induced FC
B_ext = 10 mT
Induced FC plot
B_ext = 10 mT
sample SA1
sample SA1_OX
8 times increase
M (Am²/kg)
T (K)
40 K
Magnetization M (Am²/kg)
Temperature T (K)
a)
sample SA1_OX
remanent ZFC
remanent FC
B_imprinted = 2.5 T
Remanent FC plot
B_imprinted = 2.5 T
sample SA1
sample SA1_OX
8 times increase
40 K
b)
sample SA1
sample SA1_OX
8 times increase of M_s
T = 5 K
after slope_correction
B (mT)
c)
Magnetic field induction B (T)

Table 1 Alabandite samples.

Sample	Description of sample preparation	Stoichiometry of alabandite	Stoichiometry by means of
NA	natural alabandite	$Mn_{1.007}S$	EMPA on polished speciment
SA1	solvothermal process	n.d.	
SA2	direct thermal synthesis from S and Mn powders	$MnS_{0.998}S$	SEM/ WDS on polished speciment
SA1_OX	oxidation product of sample SA1	n.d.	

n.d. stands for not determined values.

Table 2 Parameters of the hysteresis loops of (i) the NA, (ii) SA1, (iii) SA2 and (iv) SA1_OX at 5 K after the high-field slope has been subtracted.

Sample	T (K)	M_{E+} (Am^2/kg)	M_{E-} (Am^2/kg)	B_{C+} (mT)	B_{C-} (mT)	M_{R+} (Am^2/kg)	M_{R-} (Am^2/kg)
NA	5	1.910 ± 0.001	1.905 ± 0.001	424 ± 1	-608 ± 1	1.315 ± 0.001	-1.326 ± 0.001
SA1	5	0.882 ± 0.001	-0.874 ± 0.001	29 ± 1	-59 ± 1	0.344 ± 0.001	-0.225 ± 0.001
SA2	5	0.039 ± 0.001	-0.035 ± 0.001	4 ± 1	-24 ± 1	0.008 ± 0.001	-0.002 ± 0.001
SA1_OX	5	7.277 ± 0.001	7.235 ± 0.001	395 ± 1	-426 ± 1	4.564 ± 0.001	-4.376 ± 0.001

M_{E+} is the positive saturation magnetization, $M_{E–}$ is the negative saturation magnetization, B_{C+} is the positive coercivity, $B_{C–}$ is the negative coercivity, M_{R+} is the positive remanent magnetization and $M_{R–}$ is the negative remanent magnetization.